ACS Energy LETTERS

http://pubs.acs.org/journal/aelccp

Amine-Assisted Ligand-Exchange Method to Enhance Photovoltaic Parameters in $FAPbI_3$ Nanocrystal Solar Cells

Seung-Hyeon Jo,▽ Wenqiang Yang,▽ Yipeng Tang, Dong-Hyeok Kim, Wonjong Lee, Jinwoo Park, Seong Eui Chang, Sung Yeon Lim, Seongheon Kim, Yun Seog Lee, Jin Young Kim, Jongchul Lim, Bin Hu, Kai Zhu, and Tae-Woo Lee*

Cite This: *ACS Energy Lett.* 2024, 9, 2807−2815

Read Online

ACCESS | Metrics & More | Article Recommendations | Supporting Information

ABSTRACT: Perovskite colloidal nanocrystals (PeNCs) have exceptional optoelectronic properties and phase stability, making them promising for photovoltaic applications. However, insulating ligands on PeNC surfaces limit the current density and reduce the power conversion efficiency (PCE) in PeNC solar cells (SCs). This study introduces an amine-assisted ligand-exchange (ALE) strategy using 3-phenyl-1-propylamine (3P1P) to effectively remove long ligands from PeNC films. ALE reduced long-chain ligand density without increasing the number of defect states and therefore reduced the exciton-binding energy of $FAPbI_3$ NC films. These changes facilitated exciton dissociation and charge transport in $FAPbI_3$ PeNC SCs. The facilitation of exciton dissociation was due to the increased magnetic dipole interaction between excitons after the ALE process. The use of ALE achieved $FAPbI_3$ PeNC SCs that had an improved short-circuit current density of 17.98 mA/cm^2 and a PCE of 15.56% with improved stability after the treatment and negligible hysteresis. This work provides new insight into engineering PeNC films.

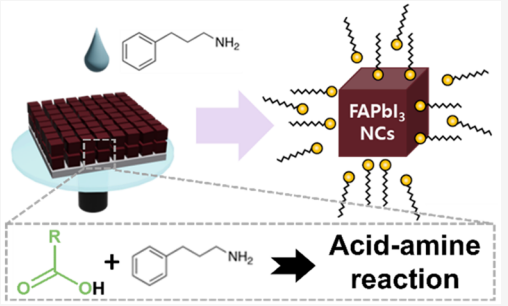

Perovskite colloidal nanocrystals (PeNCs) have high photoluminescence quantum yields (PLQYs),[1] remarkable defect tolerance,[2] and excellent photostability,[3] so they have numerous applications, including light-emitting diodes, color filters, and solar cells (SCs).[4−9] In particular, the PeNCs are gaining attention as promising candidates for SCs due to their separate crystal formation process apart from film formation processes and makes them well-suited for large-scale photovoltaic applications.[9] Additionally, the PeNCs exhibit superior phase stability compared to polycrystalline perovskite, attributed to the ligands surrounding the NCs, which have the potential to address stability concerns in polycrystalline perovskite SCs.[10] Furthermore, the PeNCs demonstrate superior photophysical properties such as slow hot carrier cooling[11] and multiple exciton generation,[12] unlike polycrystalline perovskites. These properties offer the potential to make the PCE of solar cells surpass the Schockley−Queisser limit.[13]

Long-chain alkyl (oleic acid or oleylamine) ligands are coated onto PeNCs to stabilize them in a nonpolar solvent. However, these ligands can interrupt the path for charge transport and thereby limit the power conversion efficiency (PCE) of PeNC SCs. Replacing these ligands with short ones can overcome this limitation. Most previous studies about ligand manipulation have focused on $CsPbI_3$[14−22] or FA/Cs mixed-cation PeNC SCs;[23−26] few have considered $FAPbI_3$ PeNC SCs.[10,27−29] However, $FAPbI_3$ has a narrower band gap (∼1.48 eV) than $CsPbI_3$ (∼1.73 eV)[30] and is therefore considered more suitable than $CsPbI_3$ for use in SCs. The narrow band gap increases light absorption in the perovskite films across an extended range of wavelengths. Investigations of polycrystalline perovskite SCs have been primarily focused on the $FAPbI_3$ structure.[31,32] Therefore, research on $FAPbI_3$ NC SCs should seek ways to increase their efficiency and chemical stability.

However, ligand-exchange methods that are used for $CsPbI_3$ NC SCs are not directly transferable to $FAPbI_3$ NC SCs due to the distinct properties of Cs^+ and FA^+ cations.[24] Ligand exchange on the surface of PeNCs entails a dynamic equilibrium between the adsorption and desorption of ligands

Received: April 1, 2024
Revised: April 24, 2024
Accepted: April 26, 2024

https://doi.org/10.1021/acsenergylett.4c00928
ACS Energy Lett. 2024, 9, 2807−2815

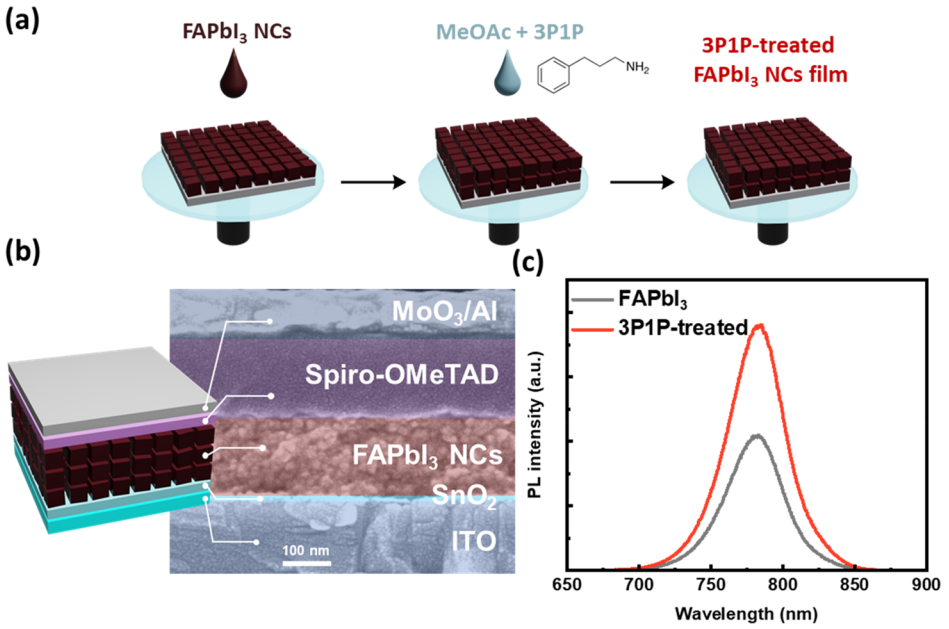

Figure 1. (a) 3P1P treatment schematics, (b) cross-section SEM image and a schematic of device structure, and (c) photoluminescence of the pristine and 3P1P-treated films.

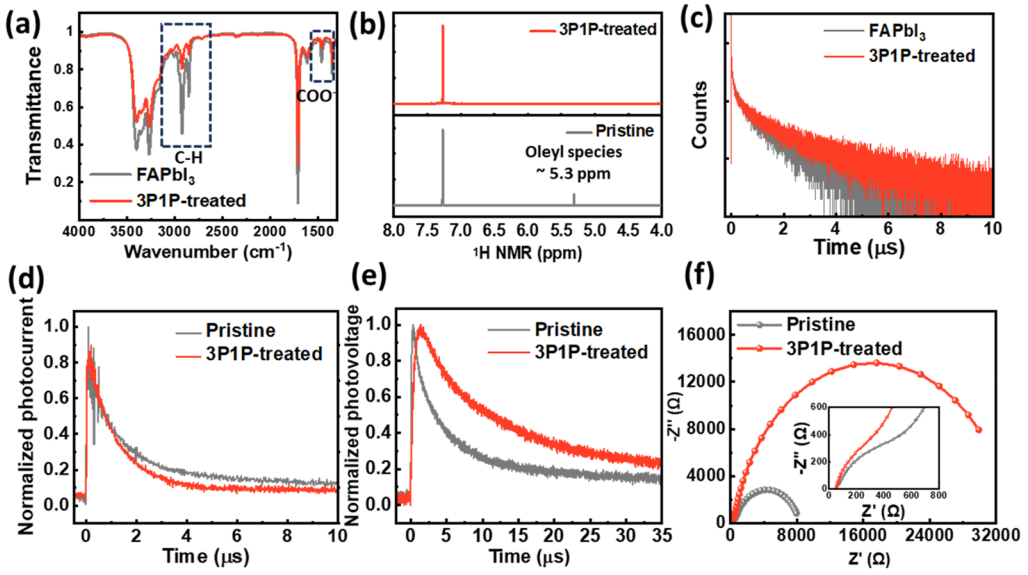

Figure 2. (a) FT-IR, (b) NMR, and (c) transient PL spectra and (d) TPC, (e) TPV, and (f) IS spectra of the pristine and 3P1P-treated films.

on PeNCs.[33] This process is susceptible to the surface chemistry of the PeNCs.

Specifically, van der Waals interactions or hydrogen bonds occur between FA^+ and ligands, but not between Cs^+ and ligands,[34] and complicate the process of manipulating ligands on $FAPbI_3$ PeNCs. Hence, to increase the PCE of $FAPbI_3$ NC SCs, alternative processes or materials tailored to the ligand exchange strategies must be developed.

In this work, we report an amine-assisted ligand-exchange (ALE) method that uses 3-phenyl-1-propylamine (3P1P) to achieve high-efficiency $FAPbI_3$ NC SCs and demonstrate its effectiveness in removing long-chain ligands. The reactivity of 3P1P with oleic acids is moderate, resulting in the removal of ligands from the NC surface without compromising stability or introducing defects. Elimination of long-chain ligands increased the short-circuit current density (J_{sc}) and fill factor (FF); these results show that the 3P1P treatment can facilitate charge transport and extraction in $FAPbI_3$ NC SCs. Furthermore, investigations of the defect status in PeNC films demonstrated that ALE did not introduce additional defects. As a result, $FAPbI_3$ NC SCs with a PCE of 15.56% were obtained.

$FAPbI_3$ PeNCs were synthesized using a hot injection method (Figure S1a, Supporting Information) that has been widely reported in the literature with minor modifications. A TEM image (Figure S1b, Supporting Information) and photoluminescence (PL)/absorbance spectrum (Figure S1c, Supporting Information) of $FAPbI_3$ NC solution were obtained. The average diameter of the $FAPbI_3$ NCs was 15.8 nm.

Ligand exchange (Figure 1a) on $FAPbI_3$ NC SCs was conducted by using a 3P1P solution. The solution was

https://doi.org/10.1021/acsenergylett.4c00928
ACS Energy Lett. 2024, 9, 2807−2815

prepared by incorporating 3P1P into methyl acetate (MeOAc), which was then used to treat the $FAPbI_3$ NC films. A layer-by-layer deposition technique was used, with sequential ligand-removing steps using MeOAc containing 3P1P alternating with pure MeOAc. The device structure schematics and cross-sectional SEM images are provided in Figure 1b.

We first examined the general properties of the film treated by 3P1P, including the optical properties, crystal structure, and surface properties. The PL (Figure 1c) spectra were obtained from pristine $FAPbI_3$ film and $FAPbI_3$ film treated with 3P1P. 3P1P treatment significantly increased the PL intensity but did not affect the PL peak position of the $FAPbI_3$ films. These results suggest that the 3P1P treatment can decrease the trap density on the surface of PeNCs. Furthermore, 3P1P treatment resulted in little change in the XRD spectra; this result indicates that this strategy would not induce degradation of the crystal structure (Figure S2, Supporting Information).

Scanning electron microscopy (SEM) images of the films (Figure S3, Supporting Information) demonstrated that the 3P1P treatment did not degrade the morphology of the $FAPbI_3$ NC film. However, atomic force microscopy (AFM) images determined that the 3P1P treatment decreased the surface roughness from 3.52 to 2.32 nm (Figure S4, Supporting Information). This decrease demonstrates that replacing the long-chain ligand with short ligands increased the packing density of PeNC films. Furthermore, X-ray photoelectron spectroscopy (XPS) analysis demonstrated that 3P1P treatment did not induce additional defects (Figure S5, Supporting Information).

To identify how the 3P1P treatment yields ligand exchange, series characterizations for PeNC films were conducted. The FT-IR spectrum changed after 3P1P treatment (Figure 2a). 3P1P treatment caused decrease in of $C-H_x$ stretching (2780−2960 cm^{-1}), C═C−H stretching (3007 cm^{-1}), and $C-H_2$ bending (1468 cm^{-1}) that are associated with oleyl groups,[35] and in symmetric stretching vibrations (1405 cm^{-1}) and asymmetric stretching vibrations (1525 cm^{-1}) that correspond to COO^- groups.[26] These results indicate that the 3P1P treatment induced an effective detachment of oleyl ligands from the $FAPbI_3$ PeNCs; this change could facilitate charge transport.

^1H NMR analysis was conducted by dispersing the PeNC films in *d*-chloroform (Figure 2b). 3P1P treatment caused a significant weakening of the signal around 5.3 ppm, which corresponds to oleyl species.[10] This change indicates that the 3P1P treatment removed long-chain ligands from the surface of the PeNCs. Two mechanisms are proposed here to explain the ligand-exchange mechanism of the 3P1P treatment. First, hydrolysis of MeOAc in the presence of water generates acetic acid and methanol.[36] By a protonation process, the acetic acid molecules replace the oleic acid ligands that are bound to the surface of the PeNCs. Second, by an acid-amine reaction, the 3P1P amine ligands react with oleic acid; this process facilitates the detachment of oleic acid ligands.[35] Removal of the long-chain ligand in PeNC film facilitates exciton dissociation and charge transport and may yield a decrease in exciton binding energy and an increase in radiative recombination time.

To gain insight into the function of amines in the ALE process, various types of amines (propylamine, PA; dipropylamine, DPA; benzylamine, BA; 3P1P) were used to treat $FAPbI_3$ NC SCs. PA is a primary alkylamine, and DPA is a secondary alkylamine. The various amines had different effects on the photovoltaic parameters of the $FAPbI_3$ NC SCs (Table S1, Supporting Information). These effects result primarily from the interaction between amine and oleic acid. The reactivity of amines with acids follows the order of secondary alkylamine > primary alkylamine > amines with phenyl groups.[35] This trend implies that amines that have excessively high reactivity with oleic acids may displace too many acid ligands from the $FAPbI_3$ NC surface and thereby increase defect density and degrade film stability. Indeed, both the V_{OC} and FF of $FAPbI_3$ NC SCs decreased after treatment with PA or DPA compared to 3P1P (Table S1, Supporting Information); this comparison indicates that defect density was higher in the films treated using PA or DPA than in those treated using 3P1P. However, treatment with BA yielded inferior photovoltaic parameters compared to treatment with 3P1P. This disparity arises from BA's weaker basicity relative to 3P1P, because of the electron-withdrawing property of phenyl groups in BA.[37] This distinction is evident in the lower J_{SC} in the BA-treated device than in the 3P1P-treated device.

Subsequently, the stability of $FAPbI_3$ NC films treated with 3P1P or DPA was compared by measuring photoluminescence (PL) and absorbance (Figure S6, Supporting Information). After exposure to amines, the films were subjected to harsh conditions (>80% relative humidity) for 18 h. In the pristine film, the PL peak shifted slightly, and the absorbance decreased; these changes indicated phase degradation of $FAPbI_3$. However, in the $FAPbI_3$ NC film that had been treated with 3P1P, the PL peak and absorbance did not change discernibly; this result indicates that PeNC films treated with 3P1P have good stability. In contrast, in the $FAPbI_3$ NC films treated with DPA, the PL peak shifted severely and the peak broadened, accompanied by a drastic decrease in absorbance. These results indicate that 3P1P amine is more suitable than DPA for treating $FAPbI_3$ NC films because 3PIP has appropriate reactivity with oleic acids.

The TrPL curve (Figure 2c) was fitted using a triexponential function to obtain estimates of each component (Table S2, Supporting Information). 3P1P treatment increased the average PL lifetime of the PeNC films from 1.0706 to 2.016 μs; this change indicates the prolongation of the radiative recombination processes.

To elucidate the recombination and transport properties of charge carriers, we performed transient photovoltage (TPV) and transient photocurrent (TPC) measurements. To calculate lifetime τ, each TPC curve (Figure 2d) and TPV curve (Figure 2e) was fitted using a stretched exponential function[38]

$$I(t) = I_0 \exp\left[-\left(\frac{t}{\tau_1}\right)^{\beta}\right] \quad (1)$$

where τ is the lifetime and β is the stretching exponent between 0 and 1. Generally, characterization techniques such as TPV and TPC can unveil the intricacies of device performance by elucidating charge carrier dynamics, encompassing both bulk and interface effects.[39] These effects are influenced by material properties and modifications, which impact phenomena, such as recombination and charge extraction. Therefore, in our study, we utilized stretched exponential decay fitting to broadly correlate material modifications with charge carrier transport dynamics. Following the 3P1P treatment, the TPV lifetime increased from 3.6 to 8.3 μs, whereas the TPC lifetime decreased from 791 to 509 ns. The prolonged lifetime of TPV signifies a diminished trap density on the surface of PeNCs, which reduces nonradiative

https://doi.org/10.1021/acsenergylett.4c00928
ACS Energy Lett. 2024, 9, 2807−2815

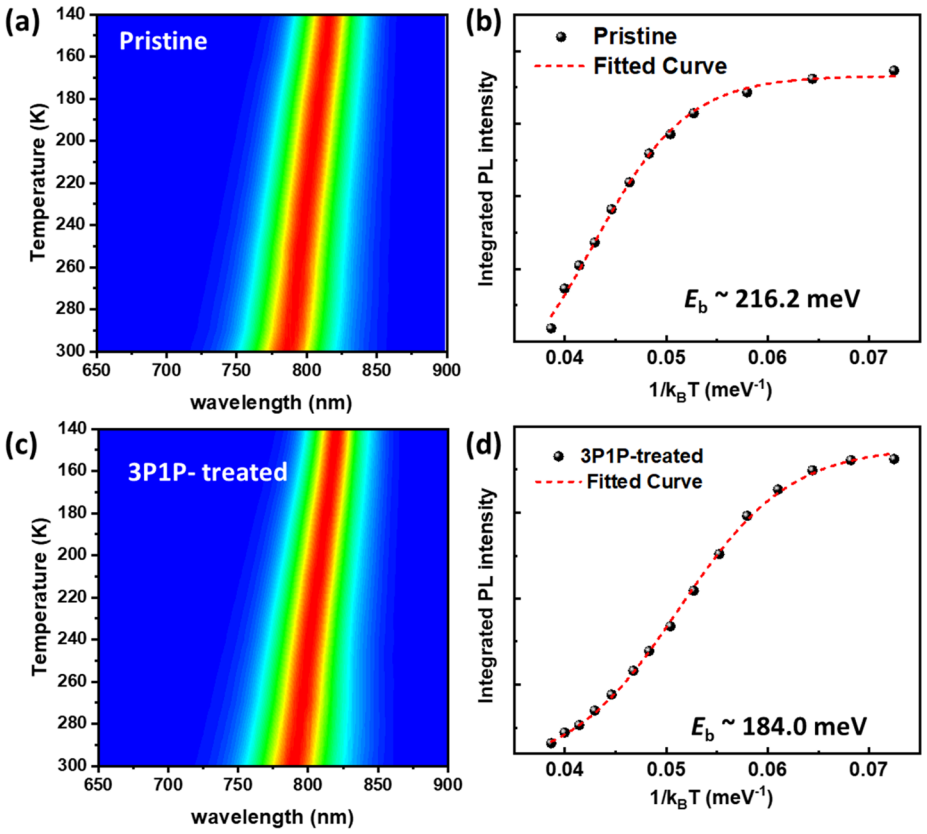

Figure 3. (a–d) Temperature-dependent PL of pristine films and 3P1P-treated films.

recombination. The shortened lifetime in the TPC curve indicates an increase in charge extraction; this change can be attributed to the decrease in the number of ligands surrounding the PeNC surface.

To gain insight into the carrier-transport ability and recombination property, we conducted impedance spectroscopy (IS) using an appropriate equivalent circuit (Figure S7, Supporting Information). The IS spectrum (Figure 2f) consists of two circles. The large one corresponds to R_{rec}, and the small one (Figure 2f inset) corresponds to R_{CT} (R_s, series resistance; R_{CT}, charge transport resistance; R_{rec}, recombination resistance).[40] 3P1P treatment decreased R_{CT} from 519.7 to 361.3 Ω but increased R_{rec} from 7586 to 33233 Ω (Table S3, Supporting Information). These findings indicate that the 3P1P treatment increased charge transport and decreased charge recombination.

We also obtained temperature-dependent PL spectra to compare the exciton binding energy, E_b, in both pristine films and those treated with 3P1P (Figure 3a–d). E_b was estimated by the integrated PL intensity to a function of $(k_BT)^{-1}$ [41]

$$I(T) = \frac{I_0}{1 + Ae^{-E_b/(k_BT)}} \tag{2}$$

where k_B is the Boltzmann constant and T is absolute temperature. Pristine films had E_b = 216.2 meV, whereas 3P1P-treated films had E_b = 184.0 meV. This decrease indicates that 3P1P treatment promotes exciton dissociation, which decreases E_b.

For a comprehensive understanding of defect-induced nonradiative recombination within the perovskite layer, we measured the effect of light intensity I on open-circuit voltage V_{OC} (Figure S8, Supporting Information). The relationship between I and V_{OC} is typically described as[42]

$$V_{OC} = \frac{nkT}{q} \ln I + C \tag{3}$$

where n is the ideality factor, k is the Boltzmann constant, q is the elementary charge, and T is the absolute temperature. n can be derived from the slope of the graph. When trap-assisted recombination is dominant, n approaches 2. Pristine devices had n = 1.6 whereas 3P1P-treated devices had n = 1.1; this decrease signifies a decrease in the number of traps in the perovskite layer.

To quantitatively analyze the trap states within the $FAPbI_3$ NC layer before and after the 3P1P treatment, we measured the space-charge-limited current (SCLC). SCLC measurement was performed on electron-only devices that had the structure ITO/SnO_2/PeNCs/PCBM/Ag. In both pristine and 3P1P-treated devices, the slope of current versus voltage was close to 1 at low voltage (Figure 4); this slope is characteristic of Ohmic contact behavior. The slope increased suddenly when the voltage exceeded the trap-filled limit voltage, V_{TFL}, at which all traps in the perovskite layer were occupied. Additionally, there was negligible hysteresis effect on forward and reverse voltage sweep. The electron trap density (n_{trap}) derived from V_{TFL} was 2.59 × 10^{17} cm^{-3} in pristine devices and 1.37 × 10^{17} cm^{-3} in 3P1P-treated devices (Table S4, Supporting Information). 3P1P treatment decreased the trap density by half; i.e., the 3P1P treatment passivated many defects. Trap density of states (tDOS) was also determined through analysis of the Mott–Schottky plot and capacitance–frequency curve (Figure S9), with detailed calculation methods provided in the Supporting Information. Notably, tDOS values were markedly

https://doi.org/10.1021/acsenergylett.4c00928
ACS Energy Lett. 2024, 9, 2807–2815

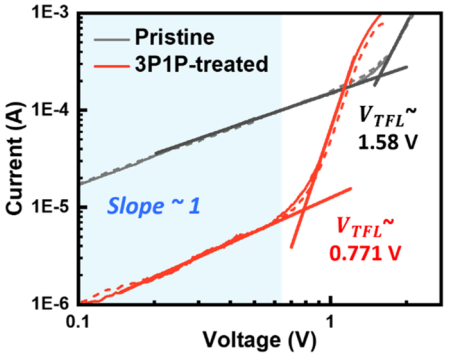

Figure 4. SCLC curve of the pristine and 3P1P-treated devices (solid line, forward scan; dashed line, reverse scan).

lower in devices treated with 3P1P compared to pristine devices, especially within the energy range of 0.3−0.45 eV (Figure S10).

To gain a thorough understanding of the exciton dynamics of 3P1P treatment which affected J_{sc} in PeNC SCs, we used photoexcitation-polarization-dependent J_{sc} measurements.[43−45] We subjected both pristine and 3P1P-treated devices to linearly and circularly polarized photoexcitation with the same intensity from a 405 nm continuous-wave laser, while monitoring J_{sc} under excitation intensities of 700 and 300 μW.

When photogenerated excitons develop an intrinsic mutual interaction between either orbital electrical polarizations or orbital magnetic dipoles, linearly and circularly polarized photoexcitations with the same intensity can inevitably generate different J_{sc}; this is the ΔJ_{sc} phenomenon. ΔJ_{sc} is defined as $\Delta J_{sc} = (J_{circular} - J_{linear})/J_{linear}$, where $J_{circular}$ and J_{linear} represent photocurrent densities under circularly and linearly polarized photoexcitation, respectively. Linearly polarized photoexcitation corresponds to antiparallel orbital magnetic dipoles with out-of-phase orbital polarization between excitons, whereas circularly polarized photoexcitation corresponds to parallel orbital magnetic dipoles with in-phase orbital polarization between excitons. Therefore, the examination of ΔJ_{sc} can help to elucidate how exciton dynamics can increase J_{sc} in PeNC SCs after surface treatment. ΔJ_{sc} provides three insights for exciton dynamics of the 3P1P treatment which increases J_{sc}.

First, circularly polarized photoexcitation of our PeNC films induced higher J_{sc} than linearly polarized photoexcitation (Figure 5a,b). This "positive-ΔJ_{sc} phenomenon" indicates that the exciton−exciton interaction intrinsically occurs through parallel orbital magnetic dipoles, which favor the generation of J_{sc} in our PeNCs.

Second, 3P1P treatment of PeNC films increased their ΔJ_{sc}; this result indicates that exciton−exciton interaction through orbital magnetic dipoles creates more excitonic states that are available to generate J_{sc}, compared to untreated PeNCs. Clearly, the surface treatment can essentially influence the exciton−exciton interaction within PeNCs.

Third, increasing photoexcitation intensity induced a larger ΔJ_{sc} in the 3P1P-treated PeNC film than in the pristine PeNC film (Figure 5c,d). This result indicates that as the exciton density increases, the J_{sc} generated by the exciton−exciton interaction also increases; this result implies that self-stimulated dissociation occurs between excitons in our surface-treated PeNCs.

The efficient ligand removal and defect passivation through the 3P1P treatment led to an increase in J_{sc} and FF in the $FAPbI_3$ PeNC solar cell, as depicted in Figure 6a. Table S5 provides a comparison of the champion photovoltaic parameters between the pristine and 3P1P-treated devices. The integrated J_{sc} calculated from the external quantum efficiency (EQE) (Figure 6b) was 16.86 mA/cm^2 in the pristine devices and 17.17 mA/cm^2 in the 3P1P-treated devices. These values differed by only ~2% from the values obtained from the $J-V$ curve, which were 16.64 mA/cm^2 in the pristine devices and 16.91 mA/cm^2 in the 3P1P-treated

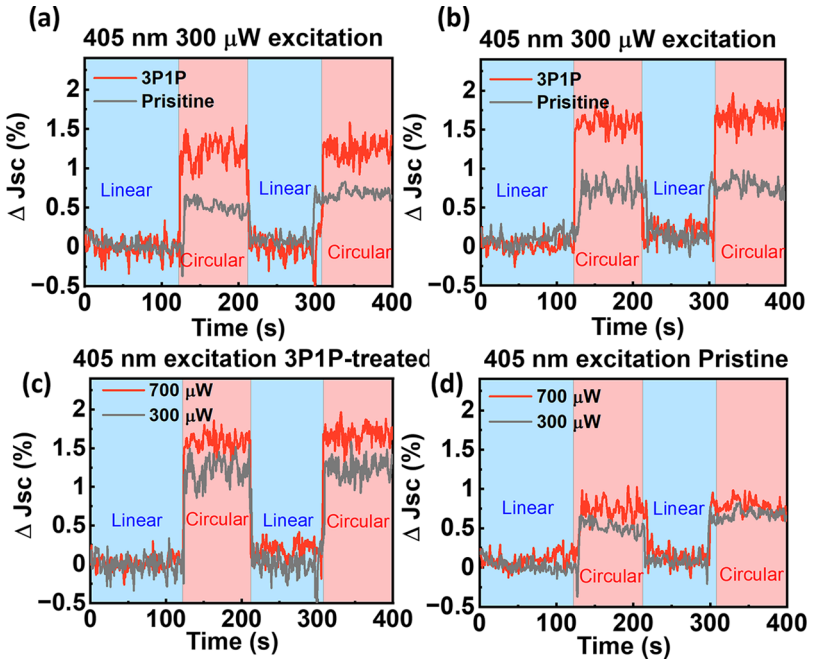

Figure 5. ΔJ_{sc} under polarized photoexcitation: (a,b) with pristine and 3P1P-treated devices, and (c,d) with different photoexcitation intensities.

https://doi.org/10.1021/acsenergylett.4c00928
ACS Energy Lett. 2024, 9, 2807−2815

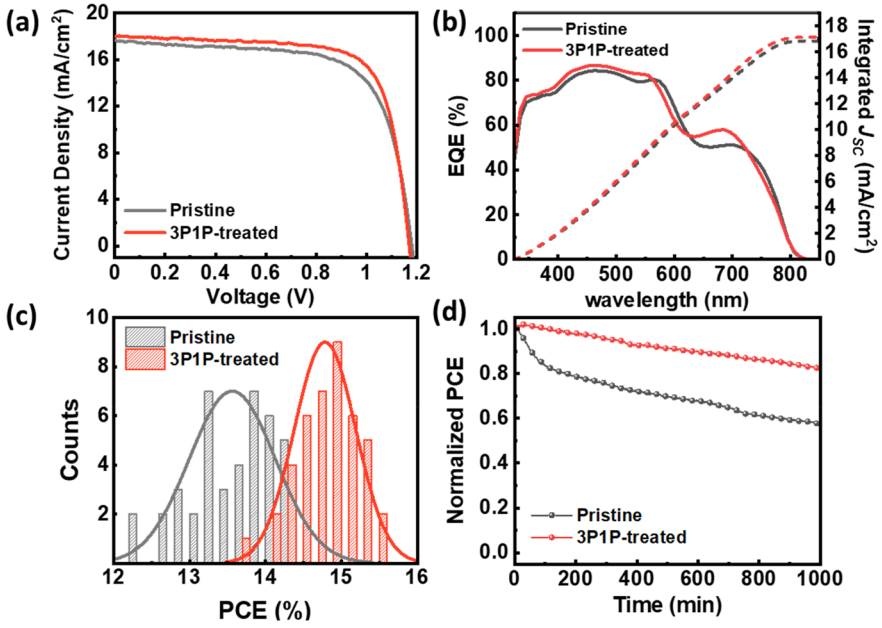

Figure 6. (a) $J-V$ curve for champion devices, (b) EQE spectrum, (c) histograms, and (d) operational stability under an N_2 atmosphere of the pristine and 3P1P-treated films.

devices. The bandgap of the $FAPbI_3$ NC films was extracted from the EQE spectrum by reported methods[46,47] (Figure S11). However, no difference in the bandgap was observed between the pristine and 3P1P-treated NC films. Hence, it can be concluded that the improved performance of the devices after treatment cannot be attributed to a change in the bandgap. Measurements on 40 devices revealed that 3P1P treatment significantly increased the average PCE of the devices (Figure 6c) and other parameters (Figure S12, Supporting Information). Moreover, devices treated with 3P1P exhibited negligible hysteresis, as evidenced by a low hysteresis index ($\frac{|PCE_{reverse} - PCE_{forward}|}{PCE_{reverse}}$) = 5%.

The 3P1P-treated devices were more stable than the pristine devices. We evaluated the operational stability of pristine and 3P1P-treated devices under 1 sun illumination (Figure 6d). Both devices were encapsulated within an N_2 atmosphere. The initial PCEs for the pristine and 3P1P-treated devices were 13.27% and 15.06%, respectively. After 1000 min, the efficiency decreased to 54% of its initial value in the pristine device, but only to 78% in the 3P1P-treated device. We also measured the storage stability of devices (Figure S13 in the Supporting Information). Both the pristine and 3P1P-treated devices were stored in dark conditions under an N_2 atmosphere with encapsulation. After 700 h, the pristine devices retained 50% of their initial PCE, whereas the 3P1P-treated devices retained 84%. These results demonstrate that the 3P1P treatment effectively increases the stability of SC devices.

In this work, we use amine-assisted ligand exchange (ALE) by using methyl acetate with 3P1P as a washing solvent for the $FAPbI_3$ NC film, to efficiently remove long-chain ligands from the surface of the PeNCs. Ligand removal by 3P1P treatment passivated the PeNC film and decreased the number of trap states and the exciton-binding energy. Consequently, charge transport and extraction properties were increased, and nonradiative recombination was decreased. The 3P1P-treated devices showed increased J_{sc} = 17.982 mA/cm^2 and PCE = 15.56%. 3P1P treatment also increased the operational and storage stability of the device. Our study demonstrates that 3P1P treatment on PeNC films is an effective strategy to increase the electrical characteristics and stability of $FAPbI_3$ PeNC SCs. This study will contribute to the further development of SCs that use $FAPbI_3$ PeNCs.

■ ASSOCIATED CONTENT

Supporting Information

The Supporting Information is available free of charge at https://pubs.acs.org/doi/10.1021/acsenergylett.4c00928.

Experimental section (including chemicals, synthesis of $FAPbI_3$ NCs, device fabrication, characterization, and tDOS calculation), Figures S1−S13, and Tables S1−S5 (PDF)

■ AUTHOR INFORMATION

Corresponding Author

Tae-Woo Lee − *Department of Materials Science and Engineering, Research Institute of Advanced Materials, School of Chemical and Biological Engineering, Institute of Engineering Research, Soft Foundry, and Interdisciplinary Program in Bioengineering, Seoul National University, Seoul 08826, Republic of Korea;* orcid.org/0000-0002-6449-6725; Email: twlees@snu.ac.kr, taewlees@gmail.com

Authors

Seung-Hyeon Jo − *Department of Materials Science and Engineering, Seoul National University, Seoul 08826, Republic of Korea*

Wenqiang Yang − *Institute of Atomic Manufacturing, International Research Institute for Multidisciplinary Science, Beihang University, Beijing 100191, People's Republic of China*

Yipeng Tang − *Department of Materials Science and Engineering, Seoul National University, Seoul 08826, Republic of Korea*

https://doi.org/10.1021/acsenergylett.4c00928
ACS Energy Lett. 2024, 9, 2807−2815

Dong-Hyeok Kim − *Department of Materials Science and Engineering, Seoul National University, Seoul 08826, Republic of Korea*
Wonjong Lee − *Graduate School of Energy Science and Technology (GEST), Chungnam National University, Daejeon 34134, Republic of Korea*
Jinwoo Park − *Department of Materials Science and Engineering, Seoul National University, Seoul 08826, Republic of Korea*
Seong Eui Chang − *Department of Materials Science and Engineering, Department of Mechanical Engineering, Research Institute of Advanced Materials, School of Chemical and Biological Engineering, Institute of Engineering Research, Soft Foundry, and Interdisciplinary Program in Bioengineering, Seoul National University, Seoul 08826, Republic of Korea; Institute of Atomic Manufacturing, International Research Institute for Multidisciplinary Science, Beihang University, Beijing 100191, People's Republic of China; Graduate School of Energy Science and Technology (GEST), Chungnam National University, Daejeon 34134, Republic of Korea; Department of Materials Science and Engineering, University of Tennessee, Knoxville TN37996, United States; Chemistry and Nanoscience Center, National Renewable Energy Laboratory, Golden, Colorado 80401, United States;* orcid.org/0009-0004-5554-0626
Sung Yeon Lim − *Department of Materials Science and Engineering, Seoul National University, Seoul 08826, Republic of Korea;* orcid.org/0009-0005-1213-4326
Seongheon Kim − *Department of Mechanical Engineering, Seoul National University, Seoul 08826, Republic of Korea*
Yun Seog Lee − *Department of Materials Science and Engineering, Seoul National University, Seoul 08826, Republic of Korea;* orcid.org/0000-0002-2289-109X
Jin Young Kim − *Department of Materials Science and Engineering, Seoul National University, Seoul 08826, Republic of Korea;* orcid.org/0000-0001-7746-9972
Jongchul Lim − *Department of Materials Science and Engineering, Department of Mechanical Engineering, Research Institute of Advanced Materials, School of Chemical and Biological Engineering, Institute of Engineering Research, Soft Foundry, and Interdisciplinary Program in Bioengineering, Seoul National University, Seoul 08826, Republic of Korea; Institute of Atomic Manufacturing, International Research Institute for Multidisciplinary Science, Beihang University, Beijing 100191, People's Republic of China; Graduate School of Energy Science and Technology (GEST), Chungnam National University, Daejeon 34134, Republic of Korea; Department of Materials Science and Engineering, University of Tennessee, Knoxville TN37996, United States; Chemistry and Nanoscience Center, National Renewable Energy Laboratory, Golden, Colorado 80401, United States;* orcid.org/0000-0001-8609-8747
Bin Hu − *Department of Materials Science and Engineering, University of Tennessee, Knoxville TN37996, United States;* orcid.org/0000-0002-1573-7625
Kai Zhu − *Chemistry and Nanoscience Center, National Renewable Energy Laboratory, Golden, Colorado 80401, United States;* orcid.org/0000-0003-0908-3909

Complete contact information is available at: https://pubs.acs.org/10.1021/acsenergylett.4c00928

Author Contributions

▽S.-H. J. and W.Y. contributed equally to this work.

Notes

The authors declare no competing financial interest.

■ ACKNOWLEDGMENTS

This work was partly supported by a Korea Institute of Energy Technology Evaluation and Planning (KETEP) grant funded by the Korean government (Ministry of Trade, Industry and Energy) (20224000000500) and the National Research Foundation of Korea (NRF) grant funded by the Korean government (Ministry of Science, ICT & Future Planning) (NRF-2016R1A3B1908431).

■ REFERENCES

(1) Dutta, A.; Behera, R. K.; Pal, P.; Baitalik, S.; Pradhan, N. Near-Unity Photoluminescence Quantum Efficiency for All CsPbX 3 (X = Cl, Br, and I) Perovskite Nanocrystals: A Generic Synthesis Approach. *Angew. Chem., Int. Ed.* **2019**, *58*, 5552−5556.
(2) du Fosse, I.; Mulder, J. T.; Almeida, G.; Spruit, A. G. M.; Infante, I.; Grozema, F. C.; Houtepen, A. J. Limits of Defect Tolerance in Perovskite Nanocrystals: Effect of Local Electrostatic Potential on Trap States. *J. Am. Chem. Soc.* **2022**, *144* (25), 11059−11063.
(3) Kim, J. I.; Zeng, Q.; Park, S.; Lee, H.; Park, J.; Kim, T.; Lee, T.-W. Strategies to Extend the Lifetime of Perovskite Downconversion Films for Display Applications. *Adv. Mater.* **2023**, *35* (43), 2209784.
(4) Lee, T.-W.; Im, S.; Kim, Y.-H.; Cho, H. Light-emitting layer for perovskite light-emitting device, method for manufacturing same, and perovskite light-emitting device using same. US10276807B2, 2019.
(5) Lee, T.-W.; Im, S.; Cho, H.; Kim, Y.-H. Perovskite light emitting device containing exciton buffer layer and method for manufacturing same. US10263207B2, 2019.
(6) Lee, T.-W.; Im, S.; Kim, Y.-H.; Cho, H. Perovskite nanocrystalline particles and optoelectronic device using same. US10193088B2, 2019.
(7) Lee, T.-W.; Im, S.; Cho, H.; Kim, Y.-H. Perovskite optoelectronic devices and method for manufacturing same. US20220199933A1, 2022.
(8) Kim, Y. H.; Kim, S.; Kakekhani, A.; Park, J.; Park, J.; Lee, Y. H.; Xu, H.; Nagane, S.; Wexler, R. B.; Kim, D. H.; Jo, S. H.; Martínez-Sarti, L.; Tan, P.; Sadhanala, A.; Park, G. S.; Kim, Y. W.; Hu, B.; Bolink, H. J.; Yoo, S.; Friend, R. H.; Rappe, A. M.; Lee, T. W. Comprehensive Defect Suppression in Perovskite Nanocrystals for High-Efficiency Light-Emitting Diodes. *Nat. Photonics* **2021**, *15* (2), 148−155.
(9) Kim, Y. H.; Park, J.; Kim, S.; Kim, J. S.; Xu, H.; Jeong, S. H.; Hu, B.; Lee, T. W. Exploiting the Full Advantages of Colloidal Perovskite Nanocrystals for Large-Area Efficient Light-Emitting Diodes. *Nat. Nanotechnol.* **2022**, *17* (6), 590−597.
(10) Xue, J.; Lee, J. W.; Dai, Z.; Wang, R.; Nuryyeva, S.; Liao, M. E.; Chang, S. Y.; Meng, L.; Meng, D.; Sun, P.; Lin, O.; Goorsky, M. S.; Yang, Y. Surface Ligand Management for Stable FAPbI3 Perovskite Quantum Dot Solar Cells. *Joule* **2018**, *2* (9), 1866−1878.
(11) Li, M.; Bhaumik, S.; Goh, T. W.; Kumar, M. S.; Yantara, N.; Grätzel, M.; Mhaisalkar, S.; Mathews, N.; Sum, T. C. Slow Cooling and Highly Efficient Extraction of Hot Carriers in Colloidal Perovskite Nanocrystals. *Nat. Commun.* **2017**, *8*, 14350.
(12) Li, M.; Begum, R.; Fu, J.; Xu, Q.; Koh, T. M.; Veldhuis, S. A.; Grätzel, M.; Mathews, N.; Mhaisalkar, S.; Sum, T. C. Low Threshold and Efficient Multiple Exciton Generation in Halide Perovskite Nanocrystals. *Nat. Commun.* **2018**, *9* (1), 4197.
(13) Kahmann, S.; Loi, M. A. Hot Carrier Solar Cells and the Potential of Perovskites for Breaking the Shockley-Queisser Limit. *J. Mater. Chem. C* **2019**, *7*, 2471−2486.
(14) Sanehira, E. M.; Marshall, A. R.; Christians, J. A.; Harvey, S. P.; Ciesielski, P. N.; Wheeler, L. M.; Schulz, P.; Lin, L. Y.; Beard, M. C.; Luther, J. M. Enhanced Mobility CsPbI 3 Quantum Dot Arrays for

Record-Efficiency, High-Voltage Photovoltaic Cells. *Sci. Adv.* **2017**, *3* (10), No. eaao4204.
(15) Swarnkar, A.; Marshall, A. R.; Sanehira, E. M.; Chernomordik, B. D.; Moore, D. T.; Christians, J. A.; Chakrabarti, T.; Luther, J. M. Quantum Dot-Induced Phase Stabilization of a-CsPbI3 Perovskite for High-Efficiency Photovoltaics. *Science* **2016**, *354* (6308), 92−95.
(16) Jia, D.; Chen, J.; Qiu, J.; Ma, H.; Yu, M.; Liu, J.; Zhang, X. Tailoring Solvent-Mediated Ligand Exchange for CsPbI3 Perovskite Quantum Dot Solar Cells with Efficiency Exceeding 16.5%. *Joule* **2022**, *6* (7), 1632−1653.
(17) Huang, H.; Zhang, X.; Gui, R.; Zhao, C.; Guo, J.; Maung, Y. M.; Yin, H.; Ma, W.; Yuan, J. High-Efficiency Perovskite Quantum Dot Photovoltaic with Homogeneous Structure and Energy Landscape. *Adv. Funct. Mater.* **2023**, *33* (13), 2210728.
(18) Hu, L.; Zhao, Q.; Huang, S.; Zheng, J.; Guan, X.; Patterson, R.; Kim, J.; Shi, L.; Lin, C. H.; Lei, Q.; Chu, D.; Tao, W.; Cheong, S.; Tilley, R. D.; Ho-Baillie, A. W. Y.; Luther, J. M.; Yuan, J.; Wu, T. Flexible and Efficient Perovskite Quantum Dot Solar Cells via Hybrid Interfacial Architecture. *Nat. Commun.* **2021**, *12* (1), 466.
(19) Han, R.; Zhao, Q.; Hazarika, A.; Li, J.; Cai, H.; Ni, J.; Zhang, J. Ionic Liquids Modulating CsPbI3 Colloidal Quantum Dots Enable Improved Mobility for High-Performance Solar Cells. *ACS Appl. Mater. Interfaces* **2022**, *14* (3), 4061−4070.
(20) Jia, D.; Chen, J.; Mei, X.; Fan, W.; Luo, S.; Yu, M.; Liu, J.; Zhang, X. Surface Matrix Curing of Inorganic CsPbI3perovskite Quantum Dots for Solar Cells with Efficiency over 16%. *Energy Environ. Sci.* **2021**, *14* (8), 4599−4609.
(21) Ling, X.; Yuan, J.; Zhang, X.; Qian, Y.; Zakeeruddin, S. M.; Larson, B. W.; Zhao, Q.; Shi, J.; Yang, J.; Ji, K.; Zhang, Y.; Wang, Y.; Zhang, C.; Duhm, S.; Luther, J. M.; Grätzel, M.; Ma, W. Guanidinium-Assisted Surface Matrix Engineering for Highly Efficient Perovskite Quantum Dot Photovoltaics. *Adv. Mater.* **2020**, *32* (26), 2001906.
(22) Khan, J.; Zhang, X.; Yuan, J.; Wang, Y.; Shi, G.; Patterson, R.; Shi, J.; Ling, X.; Hu, L.; Wu, T.; Dai, S.; Ma, W. Tuning the Surface-Passivating Ligand Anchoring Position Enables Phase Robustness in CsPbI3Perovskite Quantum Dot Solar Cells. *ACS Energy Lett.* **2020**, *5* (10), 3322−3329.
(23) Zhao, Q.; Hazarika, A.; Chen, X.; Harvey, S. P.; Larson, B. W.; Teeter, G. R.; Liu, J.; Song, T.; Xiao, C.; Shaw, L.; Zhang, M.; Li, G.; Beard, M. C.; Luther, J. M. High Efficiency Perovskite Quantum Dot Solar Cells with Charge Separating Heterostructure. *Nat. Commun.* **2019**, *10* (1), 2842.
(24) Hazarika, A.; Zhao, Q.; Ashley Gaulding, E.; Christians, J. A.; Dou, B.; Marshall, A. R.; Moot, T.; Berry, J. J.; Johnson, J. C.; Luther, J. M. Perovskite Quantum Dot Photovoltaic Materials beyond the Reach of Thin Films: Full-Range Tuning of A-Site Cation Composition. *ACS Nano* **2018**, *12* (10), 10327−10337.
(25) Hao, M.; Bai, Y.; Zeiske, S.; Ren, L.; Liu, J.; Yuan, Y.; Zarrabi, N.; Cheng, N.; Ghasemi, M.; Chen, P.; Lyu, M.; He, D.; Yun, J. H.; Du, Y.; Wang, Y.; Ding, S.; Armin, A.; Meredith, P.; Liu, G.; Cheng, H. M.; Wang, L. Ligand-Assisted Cation-Exchange Engineering for High-Efficiency Colloidal Cs1-xFAxPbI3 Quantum Dot Solar Cells with Reduced Phase Segregation. *Nat. Energy* **2020**, *5* (1), 79−88.
(26) Jia, D.; Chen, J.; Zhuang, R.; Hua, Y.; Zhang, X. Antisolvent-Assisted In Situ Cation Exchange of Perovskite Quantum Dots for Efficient Solar Cells. *Adv. Mater.* **2023**, *35* (21), 2212160.
(27) Ding, S.; Hao, M.; Fu, C.; Lin, T.; Baktash, A.; Chen, P.; He, D.; Zhang, C.; Chen, W.; Whittaker, A. K.; Bai, Y.; Wang, L. In Situ Bonding Regulation of Surface Ligands for Efficient and Stable FAPbI3 Quantum Dot Solar Cells. *Adv. Sci.* **2022**, *9* (35), 2204476.
(28) Li, F.; Zhang, X.; Shi, J.; Jin, L.; Qiao, J.; Guo, J.; Yin, H.; Li, Y.; Yuan, J.; Ma, W. Solution-Mediated Hybrid FAPbI3 Perovskite Quantum Dots for Over 15% Efficient Solar Cell. *Adv. Funct. Mater.* **2023**, *33* (40), 2302542.
(29) Li, M.; Bao, Y.; Hui, W.; Sun, K.; Gu, L.; Kang, X.; Wang, D.; Wang, B.; Deng, H.; Guo, R.; Li, Z.; Jiang, X.; Müller-Buschbaum, P.; Song, L.; Huang, W. In Situ Surface Reconstruction toward Planar Heterojunction for Efficient and Stable FAPbI3 Quantum Dot Solar Cells. *Adv. Mater.* **2024**, *36*, 2309890.
(30) Masi, S.; Gualdrón-Reyes, A. F.; Mora-Seró, I. Stabilization of Black Perovskite Phase in FAPbI3and CsPbI3. *ACS Energy Lett.* **2020**, *5* (6), 1974−1985.
(31) Yoo, J. J.; Seo, G.; Chua, M. R.; Park, T. G.; Lu, Y.; Rotermund, F.; Kim, Y. K.; Moon, C. S.; Jeon, N. J.; Correa-Baena, J. P.; Bulović, V.; Shin, S. S.; Bawendi, M. G.; Seo, J. Efficient Perovskite Solar Cells via Improved Carrier Management. *Nature* **2021**, *590* (7847), 587−593.
(32) Jeong, M.; Woo Choi, I.; Min Go, E.; Cho, Y.; Kim, M.; Lee, B.; Jeong, S.; Jo, Y.; Won Choi, H.; Lee, J.; Bae, J.-H.; Kyu Kwak, S.; Suk Kim, D.; Yang, C. Stable Perovskite Solar Cells with Efficiency Exceeding 24.8% and 0.3-V Voltage Loss. *Science* **2020**, *369* (6511), 1615−1620.
(33) Tseng, Z. L.; Chen, L. C.; Chao, L. W.; Tsai, M. J.; Luo, D.; Al Amin, N. R.; Liu, S. W.; Wong, K. T. Aggregation Control, Surface Passivation, and Optimization of Device Structure toward Near-Infrared Perovskite Quantum-Dot Light-Emitting Diodes with an EQE up to 15.4%. *Adv. Mater.* **2022**, *34* (18), 2109785.
(34) Zhang, X.; Huang, H.; Jin, L.; Wen, C.; Zhao, Q.; Zhao, C.; Guo, J.; Cheng, C.; Wang, H.; Zhang, L.; Li, Y.; Maung Maung, Y.; Yuan, J.; Ma, W. Ligand-Assisted Coupling Manipulation for Efficient and Stable FAPbI3 Colloidal Quantum Dot Solar Cells. *Angew. Chem, Int. Ed.* **2023**, *62* (5), No. e202214241.
(35) Wang, Y.; Yuan, J.; Zhang, X.; Ling, X.; Larson, B. W.; Zhao, Q.; Yang, Y.; Shi, Y.; Luther, J. M.; Ma, W. Surface Ligand Management Aided by a Secondary Amine Enables Increased Synthesis Yield of CsPbI3 Perovskite Quantum Dots and High Photovoltaic Performance. *Adv. Mater.* **2020**, *32* (32), 2000449.
(36) Wheeler, L. M.; Sanehira, E. M.; Marshall, A. R.; Schulz, P.; Suri, M.; Anderson, N. C.; Christians, J. A.; Nordlund, D.; Sokaras, D.; Kroll, T.; Harvey, S. P.; Berry, J. J.; Lin, L. Y.; Luther, J. M. Targeted Ligand-Exchange Chemistry on Cesium Lead Halide Perovskite Quantum Dots for High-Efficiency Photovoltaics. *J. Am. Chem. Soc.* **2018**, *140* (33), 10504−10513.
(37) Lévay, K.; Tóth, K. D.; Kárpáti, T.; Hegedüs, L. Heterogeneous Catalytic Hydrogenation of 3-Phenylpropionitrile over Palladium on Carbon. *ACS Omega* **2020**, *5* (10), 5487−5497.
(38) Kang, G.; Yoon, J. S.; Kim, G. W.; Choi, K.; Park, T.; Baek, R. H.; Lim, J. Electron Trapping and Extraction Kinetics on Carrier Diffusion in Metal Halide Perovskite Thin Films. *J. Mater. Chem. A* **2019**, *7* (45), 25838−25844.
(39) Krückemeier, L.; Liu, Z.; Kirchartz, T.; Rau, U. Quantifying Charge Extraction and Recombination Using the Rise and Decay of the Transient Photovoltage of Perovskite Solar Cells. *Adv. Mater.* **2023**, *35* (35), 2300872.
(40) Chen, H. W.; Huang, T. Y.; Chang, T. H.; Sanehira, Y.; Kung, C. W.; Chu, C. W.; Ikegami, M.; Miyasaka, T.; Ho, K. C. Efficiency Enhancement of Hybrid Perovskite Solar Cells with MEH-PPV Hole-Transporting Layers. *Sci. Rep.* **2016**, *6*, 34319.
(41) Zhou, N.; Huang, B.; Sun, M.; Zhang, Y.; Li, L.; Lun, Y.; Wang, X.; Hong, J.; Chen, Q.; Zhou, H. The Spacer Cations Interplay for Efficient and Stable Layered 2D Perovskite Solar Cells. *Adv. Energy Mater.* **2020**, *10* (1), 1901566.
(42) Jia, D.; Chen, J.; Zheng, S.; Phuyal, D.; Yu, M.; Tian, L.; Liu, J.; Karis, O.; Rensmo, H.; Johansson, E. M. J.; Zhang, X. Highly Stabilized Quantum Dot Ink for Efficient Infrared Light Absorbing Solar Cells. *Adv. Energy Mater.* **2019**, *9* (44), 1902809.
(43) Zhang, J.; Hu, B. Revealing Photoinduced Bulk Polarization and Spin-Orbit Coupling Effects in High-Efficiency 2D/3D Pb-Sn Alloyed Perovskite Solar Cells. *Nano Energy* **2020**, *76*, 104999.
(44) Dou, Y.; Wang, M.; Zhang, J.; Xu, H.; Hu, B. Identifying Photoinduced Dipolar Polarization and Orbit-Orbit Interaction between Excitons in Organic-Inorganic Hybrid Perovskites. *Adv. Funct. Mater.* **2020**, *30* (42), 2003476.
(45) Deng, Y.; Tai, W.; Zhang, Q.; Tang, J.; Li, J.; Wang, K.; Yu, H. High-Performance Flexible and Self-Powered Perovskite Photo-

https://doi.org/10.1021/acsenergylett.4c00928
ACS Energy Lett. 2024, 9, 2807−2815

detector Enabled by Interfacial Strain Engineering. *J. Mater. Chem. C* **2023**, *11* (2), 600−608.
(46) Almora, O.; Cabrera, C. I.; Garcia-Cerrillo, J.; Kirchartz, T.; Rau, U.; Brabec, C. J. Quantifying the Absorption Onset in the Quantum Efficiency of Emerging Photovoltaic Devices. *Adv. Energy Mater.* **2021**, *11* (16), 2100022.
(47) Caprioglio, P.; Smith, J. A.; Oliver, R. D. J.; Dasgupta, A.; Choudhary, S.; Farrar, M. D.; Ramadan, A. J.; Lin, Y. H.; Christoforo, M. G.; Ball, J. M.; Diekmann, J.; Thiesbrummel, J.; Zaininger, K. A.; Shen, X.; Johnston, M. B.; Neher, D.; Stolterfoht, M.; Snaith, H. J. Open-Circuit and Short-Circuit Loss Management in Wide-Gap Perovskite p-i-n Solar Cells. *Nat. Commun.* **2023**, *14* (1), 932.

https://doi.org/10.1021/acsenergylett.4c00928
ACS Energy Lett. 2024, 9, 2807−2815